

RXTE observations of 4U 1630–47 during the peak of its 1998 outburst

Sergey P. Trudolyubov^{1,2*}, Konstantin N. Borozdin^{2,1} and William C. Priedhorsky²

¹ *Space Research Institute, RAS, Profsoyuznaya 84/32, 117810 Moscow, Russia*

² *MS D436, Los Alamos National Laboratory, Los Alamos, 87545 New Mexico, USA*

Accepted Received in original form ??

ABSTRACT

We present an analysis of the RXTE observations of 4U 1630–47 during its outburst of 1998. The light curve and the spectral evolution of the outburst were distinctly different from the outbursts of the same source in 1996 and in 1999. Special emphasis of our analysis was on the observations taken during the initial rise of the flux and during the maximum of the outburst. The maximum of the outburst was divided into three plateaus, with almost constant flux within each plateau, and fast jumps between them. The spectral and timing parameters are stable for each individual plateau, but distinctly different between the plateaus. The variability detected on the first plateau is of special interest. During these observations the source exhibits quasi-regular modulations with period of $\sim 10 - 20$ s. Our analysis revealed significant differences in spectral and temporal behavior of the source at high and low fluxes during this period of time. The source behavior can be generally explained in the framework of the two-phase model of the accretion flow, involving a hot inner comptonization region and surrounding optically thick disk.

The variability and spectral evolution of the source were similar to what was observed earlier for other X-ray Novae. We show that 4U 1630–47 has a variety of properties which are typical for Galactic black hole binaries, both transient and persistent. We argue that this system may be an intermediate case between different groups of black hole candidates.

Key words: black hole physics – stars:binaries:general – stars:individual:4U 1630–47 – stars:novae – X-rays: general

1 INTRODUCTION

Recurrent outbursts of X-ray transient source 4U 1630–47 have been observed by X-ray experiments for thirty years. The first known outburst was recorded by Vela-5B in 1969 (Priedhorsky 1986). Multiple outbursts were detected with various all-sky monitors in later years. The outbursts occurred quasi-regularly, with a recurrence period of ~ 600 days (Jones et al. 1976; Priedhorsky 1986; Parmar, Angelini & White 1995), however, a strict regularity was ruled out by observations of several out-of-phase outbursts (Kaluzienski et al. 1978; McCollough et al. 1999).

4U 1630–47 belongs to the group of X-ray transients known as X-ray Novae (Sunyaev et al. 1994; Tanaka & Shibazaki 1996). All sources in this class are assumed to be recurrent, but only a few have been observed in more than one X-ray outburst. The typical recurrence

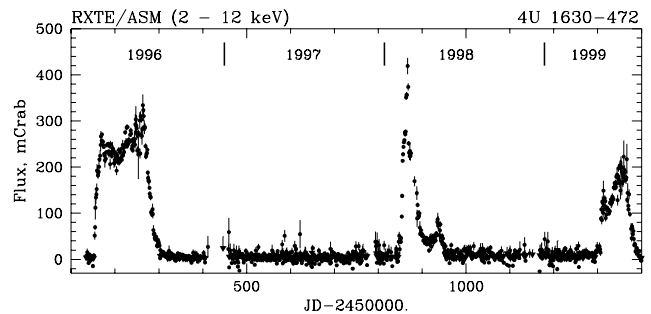


Figure 1. The long-term X-ray flux history of 4U 1630–47 according to the data of RXTE/ASM observations (each point represents daily averaged value of the X-ray flux).

time for outbursts of such sources is $\sim 10-50$ years, and 4U 1630–47, with its relatively frequent outbursts is therefore unusual. Its X-ray spectral and timing behavior during outbursts is however quite typical for

* E-mail: tsp@hea.iki.rssi.ru

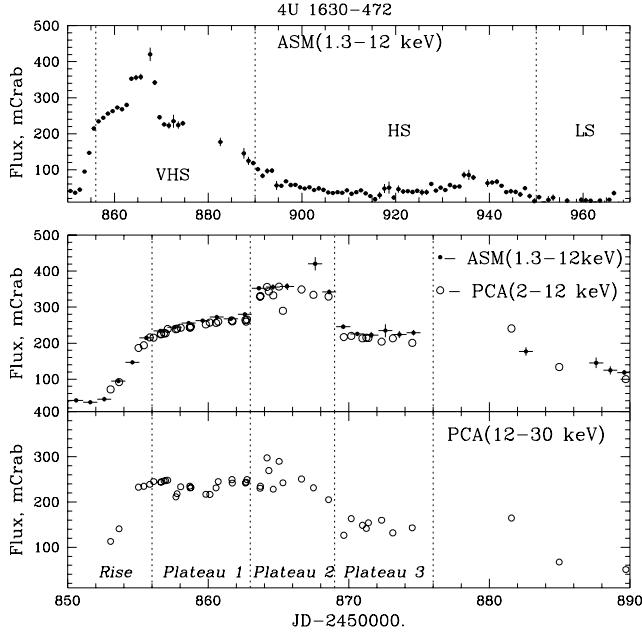


Figure 2. The light curves of 4U 1630–47 during its 1998 outburst according to the data of RXTE/PCA and ASM instruments. In upper panel general evolution of the source flux during the whole outburst is shown (1.3 – 12 keV energy band, ASM data). The detailed flux histories during the initial rise and maximum flux are shown in middle (1.3 – 12 keV energy band, ASM data – filled circles; 2 – 12 keV energy range, PCA data – hollow circles) and lower (12 – 30 keV energy range, PCA data – hollow circles) panels.

black hole binaries with low mass companions (Tanaka & Lewin 1995). No optical counterpart is known for 4U 1630–47, probably due to its high reddening and crowded field (Parmar, Stella & White 1986). Its identification as a black hole candidate in a low mass binary, derived from X-ray observations, looks nevertheless quite reliable.

The short recurrence time of the outbursts makes the source a convenient choice for studies of black hole X-ray transient behavior. In this paper we present an analysis of the observations of 4U 1630–47 during its 1998 outburst based on RXTE data. Our special emphasis was on the maximum of the outburst.

2 OBSERVATIONS AND DATA ANALYSIS

2.1 RXTE observations

RXTE satellite (Bradt, Swank, & Rothschild 1993) performed the extended series of pointed observations during 1998 outburst of 4U 1630–47. The observations started during the rise of the flux and followed the evolution of the source deep into the decline of the outburst. Total number of the observations was ~ 100 . In the Table 1 we listed observations we analyzed in detail.

For the processing of the PCA and HEXTE data we used standard RXTE FTOOLS version 4.2 tasks.

Table 1. The list of RXTE/PCA observations of 4U 1630–47 used in the analysis.

#	Obs.ID	TJD ^a	Date (UT)	Start (UT)	Exp. ^b (s)
1	30178-01-01-00	853.06	09/02/98	01:22	1034
2	30178-01-02-00	853.66	09/02/98	15:44	1134
3	30178-02-01-00	855.05	11/02/98	01:07	3554
4	30188-02-01-00	855.43	11/02/98	10:17	1175
5	30178-01-03-00	855.84	11/02/98	20:11	1438
6	30188-02-02-00	856.12	12/02/98	02:46	1846
7	30178-01-04-00	856.63	12/02/98	15:03	1659
8	30188-02-03-00	856.65	12/02/98	15:38	1509
9	30178-02-01-01	856.87	12/02/98	20:51	2919
10	30188-02-04-00	856.98	12/02/98	23:26	2015
11	30178-01-05-00	857.12	13/02/98	02:47	1441
12	30188-02-05-00	857.71	13/02/98	17:01	2266
13	30178-02-02-00	857.79	13/02/98	19:02	6540
14	30188-02-06-00	858.05	14/02/98	01:05	2168
15	30178-01-06-00	858.70	14/02/98	16:40	1453
16	30188-02-07-00	858.72	14/02/98	17:10	1786
17	30178-02-02-01	858.77	14/02/98	18:31	8414
18	30178-01-07-00	859.84	15/02/98	20:04	1370
19	30188-02-08-00	860.12	16/02/98	02:48	1828
20	30188-02-09-00	860.56	16/02/98	13:29	1597
21	30178-01-08-00	860.72	16/02/98	17:20	1180
22	30178-01-09-00	861.69	17/02/98	16:38	1314
23	30188-02-10-00	861.72	17/02/98	17:21	1620
24	30178-01-10-00	862.65	18/02/98	15:41	1638
25	30188-02-11-00	862.71	18/02/98	16:54	2864
26	30178-02-03-00	862.77	18/02/98	18:22	9296
27	30178-01-11-00	863.70	19/02/98	16:41	1237
28	30188-02-12-00	863.71	19/02/98	17:06	2245
29	30188-02-13-00	864.19	20/02/98	04:26	1233
30	30188-02-14-00	864.32	20/02/98	07:41	1080
31	30178-01-12-00	864.63	20/02/98	15:07	1579
32	30188-02-15-00	865.05	21/02/98	01:06	1510
33	30188-02-16-00	865.32	21/02/98	07:41	912
34	30188-02-17-00	866.64	22/02/98	15:21	1419
35	30178-01-13-00	867.50	23/02/98	11:56	1524
36	30188-02-18-00	868.57	24/02/98	13:38	3620
37	30188-02-19-00	869.65	25/02/98	15:37	1698
38	30188-02-20-00	870.18	26/02/98	04:21	900
39	30178-01-14-00	870.98	26/02/98	23:28	1895
40	30188-02-21-00	871.26	27/02/98	06:11	2175
41	30188-02-21-01	871.41	27/02/98	09:50	772
42	30188-02-22-00	872.34	28/02/98	08:12	4972
43	30188-02-23-00	873.14	01/03/98	03:19	1347
44	30178-01-15-00	874.52	02/03/98	12:23	1400
45	30178-01-16-00	881.58	09/03/98	13:55	1875
46	30178-01-17-00	884.94	12/03/98	22:33	1590
47	30178-01-18-00	889.72	17/03/98	17:08	1359
48	30172-01-05-00	891.65	19/03/98	15:30	9152

^a – Truncated Julian Date: TJD=JD-2450000.

^b – Dead time corrected value of the PCA exposure

2.2 Spectral analysis

For the spectral analysis we used PCA data collected in the 3 – 20 keV energy range. PCA response matrixes for individual observations were constructed using PCARMF v3.5, background estimation was performed applying a Very-Large Events (VLE)–based model. To evaluate correct source flux, the standard dead time correction procedure was applied to the PCA

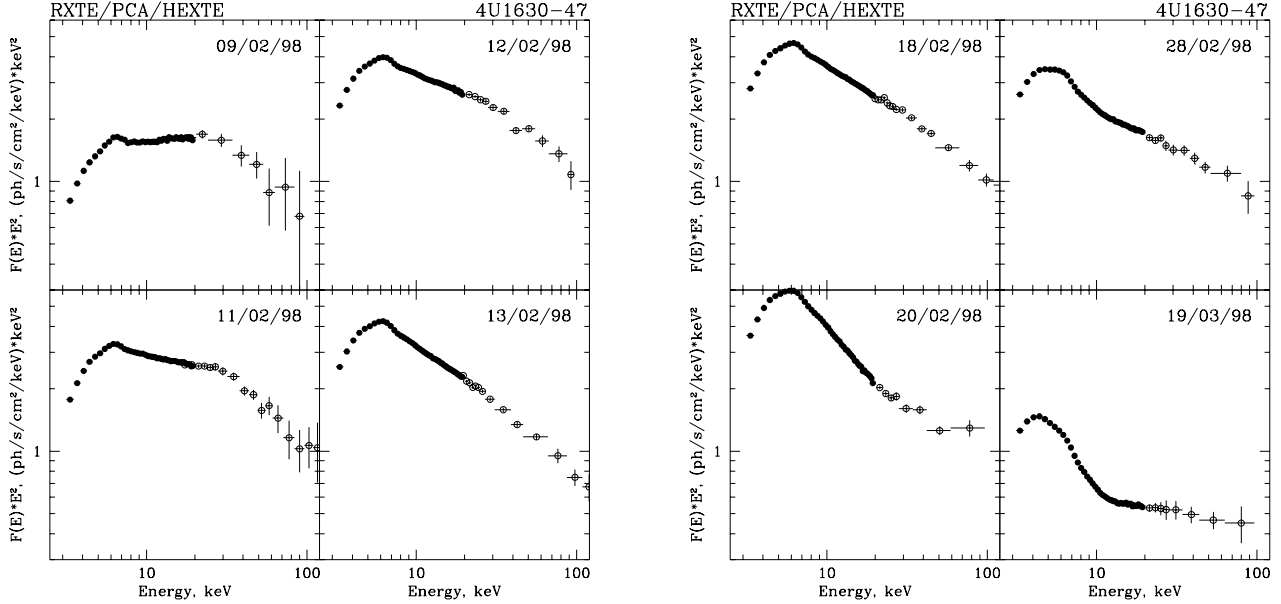


Figure 3. Typical broad-band spectra of 4U1630-47 during the initial rise and maximum phase of the 1998 outburst. Filled and hollow circles represent the data of PCA and HEXTE instruments respectively.

data. In order to account for the uncertainties of the response matrix, a 1% – systematic error was added to the statistical error for each PCA energy channel.

We used the HEXTE response matrices, released on April 3, 1997 and standard off-source observations for each cluster of detectors to subtract background. In order to account for the uncertainties in the response and background determination, only data in the 19–100 keV energy range were taken for the spectral analysis.

We generated the energy spectra of 4U 1630-47 averaging the data over the whole single observations using the *Standard2* mode data. To trace the evolution of the source spectral properties on the short time scales the data in the *Binned* and *Event* modes were used.

As we are interested in the general character of the 4U 1630-47 spectral evolution, we used only simplest models to approximate its spectra. Due to the cross-calibration uncertainties the data of PCA and HEXTE instruments were analyzed separately. For the approximation of the PCA spectral data a sum of the XSPEC “multicolor disk black body” model[†] and a power law model, corrected for the interstellar absorption were used. Although this model provides satisfactory description to the overall shape of the spectrum, sometimes there is a significant excess of emission in the 6 – 8 keV

region (with an average ratio of excess to the model continuum of $\sim 1-3\%$), which is attributed to the presence of the iron emission/absorption complex. Due to the relatively low energy resolution of the PCA instrument ($\Delta E \sim 1$ keV in the 6 – 8 keV range) it is not possible to carry out a detailed analysis of this spectral feature. The presence of the iron emission/absorption features shows the evidence for the additional ‘reprocessed’ component in the source spectrum, but its approximation by certain type of model requires further physical justification, so we have decided not to include ‘reprocessed’ component to the fit.[‡] For the analytic approximation of the HEXTE data a simple power model was used.

Typical examples of the broad-band energy spectra of 4U 1630-47 in units of $E^2 \times F(E)$ (keV² phot/keV) are shown in Fig. 3. The results of fitting of the PCA and HEXTE spectral data with analytical models described above are presented in Table 2. Figure 4 shows the evolution of fitting parameters with time.

2.3 Timing analysis

For the timing analysis the PCA *Binned*, *Single Binned* and *Event* mode data were used. We generated power density spectra (PDS) in the 0.001–256 Hz frequency range (2–13 keV energy band), combining the results of the summed Fourier transforms of a short stretches

[†] Note that no corrections for the electron scattering and effects of general relativity were made (Shakura & Sunyaev 1973; Shimura & Takahara 1995). In addition, this model assumes incorrect radial dependence of the disk effective temperature within ~ 5 gravitational radii. Thus the inferred value of the effective radius R_{in} should not be treated as the actual value of the characteristic radius of the optically thick emitting region

[‡] The inclusion of Gaussian emission line and absorption edge model features has minor effect on the values of the main model parameters and integrated energy flux, derived through the spectral fitting, except for the value of color temperature T_d of the soft component, which decreases by $\sim 20\%$

Table 2. Spectral parameters of 4U 1630-47, derived using the combination of the multicolor disc blackbody (Mitsuda et al. 1984) and power law models with correction to the interstellar absorption (PCA data, 3 – 20 keV energy range). Parameter errors correspond to 1 σ confidence level for the assumed 1% systematic uncertainty of data. For the approximation of HEXTE data in the 19 – 100 keV energy range a simple power law model was used. In order to improve statistical significance the data of HEXTE instrument were averaged over several observations corresponding to the same date.

#	T _d , keV	Norm ^a	f _{soft} ^{bol b}	α_{pl}	N _H ^c	f _{total} ^d	f _{soft} ^e	$\chi^2(\text{d.o.f.})$	α_{pl}^f
1	1.88 ± 0.06	6.0 ± 0.7	1.63	1.73 ± 0.06	7.22 ± 0.37	4.13	0.91	63.5(40)	2.46 ± 0.07
2	1.76 ± 0.06	8.1 ± 1.2	1.66	1.85 ± 0.05	7.48 ± 0.35	5.32	0.88	59.5(40)	2.55 ± 0.13
3	1.73 ± 0.05	17.6 ± 2.0	3.42	2.09 ± 0.04	7.84 ± 0.31	10.50	1.78	21.7(40)	2.51 ± 0.04
4	1.72 ± 0.06	18.2 ± 2.3	3.48	2.12 ± 0.05	7.71 ± 0.35	10.80	1.81	30.4(40)	
5	1.68 ± 0.04	25.9 ± 2.9	4.49	2.18 ± 0.04	8.05 ± 0.32	11.94	2.29	15.7(40)	
6	1.68 ± 0.05	24.3 ± 2.7	4.17	2.17 ± 0.04	7.78 ± 0.32	11.88	2.12	17.7(40)	2.51 ± 0.03
7	1.69 ± 0.05	23.3 ± 2.8	4.08	2.25 ± 0.04	8.08 ± 0.33	12.47	2.08	26.5(40)	
8	1.68 ± 0.04	24.0 ± 3.0	4.09	2.24 ± 0.04	7.90 ± 0.33	12.33	2.07	23.7(40)	
9	1.66 ± 0.05	23.9 ± 2.1	3.94	2.26 ± 0.03	7.97 ± 0.31	12.57	1.98	25.4(40)	
10	1.64 ± 0.05	23.2 ± 3.3	3.63	2.28 ± 0.03	8.13 ± 0.32	12.60	1.80	19.0(40)	
11	1.69 ± 0.03	32.0 ± 3.0	5.60	2.21 ± 0.04	7.88 ± 0.32	13.01	2.85	21.2(40)	2.71 ± 0.02
12	1.68 ± 0.03	32.8 ± 3.0	5.65	2.40 ± 0.04	8.35 ± 0.33	12.88	2.87	20.2(40)	
13	1.68 ± 0.03	30.1 ± 2.9	5.13	2.41 ± 0.03	8.38 ± 0.32	13.06	2.60	18.6(40)	
14	1.69 ± 0.04	30.1 ± 2.9	5.30	2.32 ± 0.04	8.03 ± 0.33	13.12	2.71	21.3(40)	2.70 ± 0.02
15	1.69 ± 0.04	25.8 ± 3.2	4.53	2.37 ± 0.04	8.22 ± 0.34	13.30	2.31	22.7(40)	
16	1.70 ± 0.04	26.8 ± 3.0	4.87	2.36 ± 0.04	8.03 ± 0.34	13.12	2.50	23.9(40)	
17	1.68 ± 0.03	28.7 ± 2.9	4.90	2.38 ± 0.03	8.23 ± 0.30	13.37	2.48	17.1(40)	
18	1.72 ± 0.03	25.1 ± 3.3	4.72	2.52 ± 0.04	8.83 ± 0.36	13.81	2.44	26.4(40)	2.57 ± 0.06
19	1.71 ± 0.03	32.2 ± 3.3	5.92	2.47 ± 0.04	8.56 ± 0.35	13.92	3.05	19.8(40)	2.70 ± 0.06
20	1.68 ± 0.04	28.0 ± 3.3	4.85	2.44 ± 0.04	8.31 ± 0.34	13.87	2.47	26.4(40)	
21	1.70 ± 0.04	29.2 ± 3.2	5.22	2.35 ± 0.04	7.81 ± 0.35	13.91	2.68	26.8(40)	
22	1.72 ± 0.04	24.0 ± 3.3	4.48	2.41 ± 0.04	8.32 ± 0.36	14.34	2.32	21.6(40)	2.57 ± 0.07
23	1.70 ± 0.04	28.0 ± 3.1	5.07	2.38 ± 0.04	8.02 ± 0.34	14.00	2.60	19.7(40)	
24	1.71 ± 0.04	28.9 ± 3.1	5.31	2.39 ± 0.04	8.02 ± 0.34	14.17	2.73	22.9(40)	2.60 ± 0.02
25	1.68 ± 0.04	29.6 ± 3.1	5.14	2.38 ± 0.04	8.10 ± 0.33	14.03	2.62	21.2(40)	
26	1.69 ± 0.04	26.3 ± 3.0	4.69	2.42 ± 0.04	8.38 ± 0.32	14.51	2.40	19.8(40)	
27	1.73 ± 0.02	55.0 ± 3.9	10.53	2.54 ± 0.05	8.70 ± 0.36	17.39	5.48	19.7(40)	2.76 ± 0.04
28	1.72 ± 0.02	53.2 ± 3.8	10.05	2.57 ± 0.04	8.97 ± 0.35	17.77	5.21	21.0(40)	
29	1.82 ± 0.03	35.2 ± 3.7	8.33	2.48 ± 0.05	8.77 ± 0.37	19.37	4.53	27.1(40)	2.50 ± 0.07
30	1.81 ± 0.03	37.6 ± 3.7	8.76	2.52 ± 0.05	8.69 ± 0.37	18.46	4.75	21.0(40)	
31	1.75 ± 0.02	48.4 ± 4.0	9.70	2.63 ± 0.05	9.12 ± 0.37	17.89	5.09	25.1(40)	
32	1.82 ± 0.03	37.2 ± 3.6	8.91	2.49 ± 0.05	8.77 ± 0.36	19.32	4.86	27.2(40)	2.69 ± 0.05
33	1.72 ± 0.03	31.0 ± 3.9	5.86	2.50 ± 0.05	8.36 ± 0.37	15.55	3.04	28.2(40)	2.58 ± 0.05
34	1.80 ± 0.02	43.6 ± 3.8	9.78	2.59 ± 0.05	8.97 ± 0.37	18.76	5.26	25.6(40)	2.60 ± 0.06
35	1.76 ± 0.02	49.3 ± 3.7	10.15	2.58 ± 0.05	8.75 ± 0.36	17.71	5.36	20.7(40)	2.69 ± 0.06
36	1.69 ± 0.02	58.8 ± 3.9	10.43	2.69 ± 0.04	8.95 ± 0.34	17.43	5.33	26.4(40)	2.68 ± 0.04
37	1.31 ± 0.02	188.1 ± 13.1	11.78	2.39 ± 0.04	6.87 ± 0.27	10.51	4.54	27.6(40)	2.12 ± 0.20
38	1.30 ± 0.03	147.8 ± 14.7	9.04	2.36 ± 0.04	6.94 ± 0.31	11.03	3.45	23.8(40)	2.40 ± 0.06
39	1.30 ± 0.02	167.8 ± 13.7	10.35	2.31 ± 0.03	6.97 ± 0.27	10.61	3.97	23.8(40)	
40	1.30 ± 0.02	171.3 ± 13.1	10.71	2.35 ± 0.03	6.94 ± 0.27	10.61	4.12	17.9(40)	2.42 ± 0.05
41	1.31 ± 0.03	151.7 ± 15.1	9.67	2.30 ± 0.04	6.64 ± 0.30	10.57	3.74	31.7(40)	
42	1.31 ± 0.02	133.8 ± 12.7	8.43	2.26 ± 0.03	6.51 ± 0.28	10.12	3.25	18.2(40)	2.42 ± 0.04
43	1.33 ± 0.02	169.2 ± 12.2	11.55	2.30 ± 0.04	6.77 ± 0.27	10.35	4.57	15.1(40)	2.39 ± 0.08
44	1.29 ± 0.02	151.6 ± 14.3	9.08	2.32 ± 0.03	6.58 ± 0.28	9.85	3.45	23.8(40)	2.43 ± 0.07
45	1.59 ± 0.02	70.5 ± 3.9	9.63	2.42 ± 0.04	7.60 ± 0.30	12.17	4.63	31.2(40)	2.37 ± 0.05
46	1.24 ± 0.02	191.1 ± 12.4	9.78	2.17 ± 0.04	6.06 ± 0.26	6.15	3.52	23.1(40)	2.20 ± 0.16
47	1.20 ± 0.02	174.5 ± 12.2	7.90	2.05 ± 0.05	5.74 ± 0.28	4.54	2.73	39.0(40)	2.05 ± 0.16
48	1.21 ± 0.02	112.1 ± 7.8	5.15	2.05 ± 0.03	4.74 ± 0.25	3.53	1.78	28.6(40)	2.19 ± 0.06

^a – normalization of the soft spectral component $N_{\text{diskbb}} = \left(\frac{R_{\text{in}}(\text{km})}{D_{10\text{kpc}}} \right)^2 \cos(\theta)$, where $R_{\text{in}}(\text{km})$ – effective inner radius of the disk, $D_{10\text{kpc}}$ – source distance in units of 10 kpc, θ – inclination angle of the accretion disk

^b – bolometric flux of the soft spectral component in units of $\times 10^{-9} \text{ erg s}^{-1} \text{ cm}^{-2}$

^c – equivalent hydrogen column density in units of $\times 10^{22} \text{ cm}^{-2}$

^d – absorption corrected value of the total X-ray flux in the 3 – 20 keV energy range in units of $\times 10^{-9} \text{ erg s}^{-1} \text{ cm}^{-2}$

^e – absorption corrected value of the soft spectral component flux in the 3 – 20 keV energy range in units of $\times 10^{-9} \text{ erg s}^{-1} \text{ cm}^{-2}$

^f – photon index of hard spectral component derived from fitting of the HEXTE data.

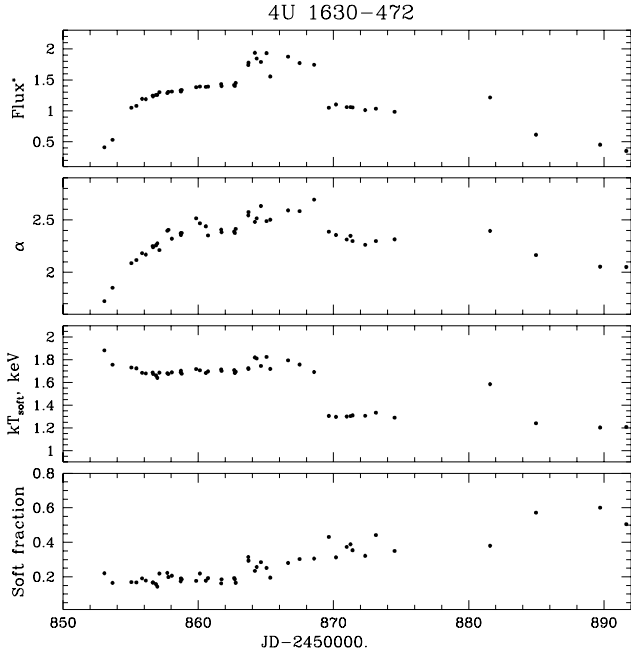


Figure 4. The evolution of the spectral parameters of the multicolor disk black body plus power law model approximation for energy spectra of 4U1630-47 during the 1998 outburst. 'Soft fraction' denotes the ratio of the flux of component to the total flux from the source in the 3 – 20 keV energy range. 'Flux*' denotes the total model flux in the 3–20 keV energy range corrected for the low energy absorption (in units of $\times 10^{-8}$ erg/s/cm²).

of data with 0.002 s time bins for the 0.3 – 128 Hz frequency range and a single Fourier transform on the data in 0.125 s time bins for lower frequency band. The resulting spectra were logarithmically rebinned when necessary to reduce scatter at high frequencies and normalized to square root of fractional variability rms. White-noise level due to the Poissonian statistics corrected for the dead-time effects was subtracted (Vikhlinin, Churazov & Gilfanov 1994; Zhang et al. 1995).

To trace the evolution of the source timing properties, we fitted its power density spectra in the 0.01 – 100 Hz frequency range to the analytic models using the χ^2 minimization technique. For the approximation of the PDS obtained during the first 26 observations the combination of the band-limited noise (BLN) component (approximated by zero-centered Lorentzian function) and several quasi-periodic oscillations (QPO) (expressed by Lorentzian functions) was used. Beginning on the observation #27 (except for the observation #33) an additional power law component expressing the Very Low Frequency Noise (VLFN) component is required.

Typical examples of the broad-band power density spectra of 4U 1630-47 during the 1998 outburst are shown in Fig. 5 (for the convenience, PDS are presented in units of $f \times (\text{rms}/\text{mean})^2/\text{Hz}$, representing the actual distribution of the variability amplitude over frequency). General parameters of the source power density spectra and their evolution during the outburst are presented in Table 3 and Figure 6 respectively.

Table 3. The characteristics of the power density spectra of 4U 1630-47. Parameter errors correspond to 1σ confidence level. $\text{rms}_{\text{total}}$ represents total rms amplitude integrated over 0.02 – 100 Hz frequency range, f_{QPO} and rms_{QPO} represent the centroid frequency and the rms amplitude of the Lorentzians used to approximate the QPO peaks.

Date, UT	#	$\text{rms}_{\text{total}}, \%$	$f_{\text{QPO}}, \text{Hz}$	$\text{rms}_{\text{QPO}}, \%$
09/02/98	(1)	27.97 ± 0.24	2.68 ± 0.01	14.84 ± 0.90
			5.60 ± 0.07	4.83 ± 0.33
09/02/98	(2)	25.47 ± 0.18	3.21 ± 0.01	14.08 ± 0.80
			6.54 ± 0.08	3.93 ± 0.30
11/02/98	(3-5)	12.34 ± 0.09	3.82 ± 0.02	4.85 ± 0.30
			7.77 ± 0.06	4.79 ± 0.30
12/02/98	(6-10)	10.83 ± 0.05	4.80 ± 0.01	4.44 ± 0.19
			7.97 ± 0.09	3.80 ± 0.35
13/02/98	(11-13)	10.71 ± 0.05	0.079 ± 0.002^1	4.19 ± 0.49
			4.74 ± 0.06	2.61 ± 0.17
			7.05 ± 0.03	3.62 ± 0.11
			13.59 ± 0.08	1.99 ± 0.14
14/02/98	(14-17)	10.56 ± 0.04	0.094 ± 0.002^1	3.03 ± 0.48
			5.38 ± 0.04	4.53 ± 0.16
			7.75 ± 0.13	2.68 ± 0.28
			13.29 ± 0.07	1.97 ± 0.13
			0.067 ± 0.005^1	3.77 ± 0.89
15/02/98	(18)	10.10 ± 0.19	4.69 ± 0.07	2.07 ± 0.29
			7.07 ± 0.04	3.52 ± 0.25
			13.20 ± 0.50	1.95 ± 0.40
			4.87 ± 0.07	2.56 ± 0.22
			6.94 ± 0.06	3.44 ± 0.16
16/02/98	(19-21)	9.89 ± 0.10	13.35 ± 0.15	1.87 ± 0.20
			0.097 ± 0.002^1	3.28 ± 0.84
			5.23 ± 0.09	2.67 ± 0.47
			6.62 ± 0.39	4.69 ± 1.04
			13.83 ± 0.34	1.51 ± 0.50
18/02/98	(24-26)	10.24 ± 0.05	0.091 ± 0.002^1	3.53 ± 0.32
			5.03 ± 0.06	3.23 ± 0.29
			6.89 ± 0.15	3.94 ± 0.35
			13.31 ± 0.10	1.77 ± 0.12
			7.04 ± 0.28	1.32 ± 0.26
19/02/98	(27-28)	2.13 ± 0.23	12.56 ± 0.85	1.43 ± 0.30
			–	–
20/02/98	(29-31)	1.93 ± 0.20	–	–
21/02/98	(32)	2.74 ± 0.37	–	–
21/02/98	(33)	10.16 ± 0.32	0.052 ± 0.010^1	2.79 ± 0.83
			4.45 ± 0.16	1.88 ± 0.40
			7.04 ± 0.06	3.05 ± 0.30
			12.25 ± 0.73	1.40 ± 0.63
22/02/98	(34)	2.43 ± 0.50	–	–
23/02/98	(35)	3.09 ± 0.16	–	–
24/02/98	(36)	3.53 ± 0.49	9.50 ± 1.65	1.85 ± 0.45
25/02/98	(37)	3.99 ± 0.17	10.93 ± 0.83	1.75 ± 0.43
26/02/98	(38-39)	3.61 ± 0.44	11.19 ± 0.43	1.86 ± 0.34
27/02/98	(40-41)	4.27 ± 0.19	10.33 ± 0.44	1.78 ± 0.30
28/02/98	(42)	3.74 ± 0.27	10.99 ± 0.13	1.84 ± 0.22
01/03/98	(43)	2.20 ± 0.58	10.76 ± 0.59	1.77 ± 0.47
02/03/98	(44)	1.98 ± 0.69	11.12 ± 0.39	1.62 ± 0.37
09/03/98	(45)	1.93 ± 0.48	7.87 ± 0.26	1.67 ± 0.39
12/03/98	(46)	1.80 ± 0.50	–	–
17/03/98	(47)	1.96 ± 0.75	–	–
19/03/98	(48)	1.74 ± 0.31	–	–

¹ – the QPO peak shows harmonic content

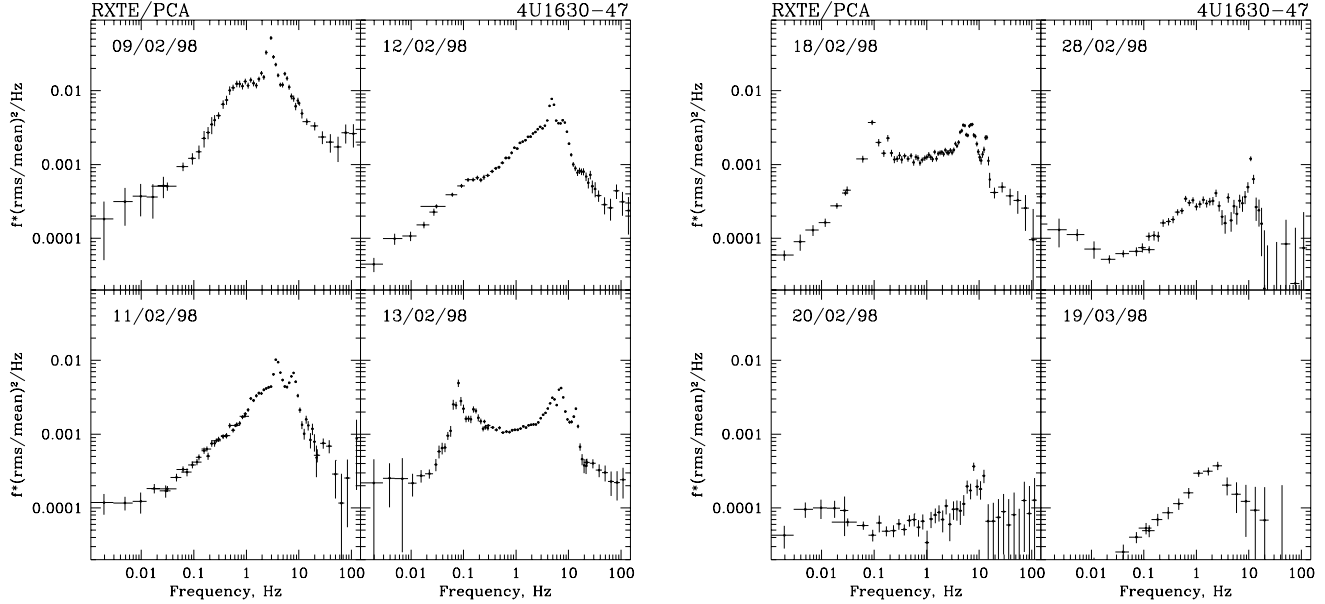


Figure 5. Typical broad-band power density spectra of 4U1630-47 in units of $f \times (\text{rms}/\text{mean})^2/\text{Hz}$ during the initial rise and maximum phase of the 1998 outburst. 2 – 13 keV energy band, PCA data.

3 LIGHT CURVE OF 4U 1630-47

In four years RXTE satellite detected three outbursts from 4U 1630-47 (Fig. 1). The beginning of 1998 outburst was predicted by Kuulkers et al. (1997) with an accuracy of few days. This prediction was based on the time of the 1996 outburst, and the mean period over the epoch 1987-1996. However, the outburst of 1999 occurred much earlier than was expected from both the interval of ~ 690 days suggested by Kuulkers et al. (1997), and from earlier calculated recurrence interval 602 ± 3 days (Parmar, Angelini & White 1995). Because the recurrence time of the outbursts appears not to be absolutely stable, we suggest that this time is not linked to the parameters of binary orbit, but instead is due to the typical time of mass collection in the accretion disk. Recurrent outbursts with typical time 440 ± 30 days were observed from another Galactic black hole candidate GX 339-4 in 1991-1994 (Harmon et al. 1994), but later the recurrence was broken. In case of GX 339-4 the orbital period was measured to be 14.8 h (Callanan et al. 1992).

The three outbursts differ significantly in their shape. While the outbursts of 1996 and 1999 years remind low/high state transitions in persistent X-ray sources as Cyg X-1 (Cui et al. 1998) and GX339-4 (Belloni et al. 1999), 1998 outburst was of fast-rise-exponential-decay (FRED) type typical for many X-ray Novae (Chen, Shrader & Livio 1997).

The light curve of the 1998 outburst presented in more detail in Fig. 2. The flux from 4U1630-47 rose for about 5 days before reaching the level of about 200 mCrab. The maximum of the outburst was composed of three plateaus with almost constant flux at each plateau

and fast jumps between them. The second plateau was the highest one with maximum flux above 400 mCrab. The duration of each plateau was 6-7 days. A month after the beginning of the outburst quasi-exponential decline started, with secondary maxima, as typical for many X-ray transients.

4 EVOLUTION OF THE SOURCE DURING THE OUTBURST OF 4U 1630-47

During 1998 outburst the source demonstrated a variety of different spectral and timing states. Thanks to good coverage of the outburst by RXTE pointing observations we had an opportunity to study the changes in detail. A summary of the states observed is presented in Table 4.

4.1 The rise of the outburst

RXTE pointed observations started at Feb 9, 1998, a week after the beginning of the outburst detected by ASM/RXTE. Several PCA and HEXTE observations were carried out when the source was still in the rise phase. The broad-band energy spectrum of 4U1630-47 during these observations (##1-5) can be generally described by sum of a strong hard component approximated by a power law model with a photon index $\sim 1.8 - 2.2$ and a high energy cut-off at $\sim 60 - 70$ keV and a weak soft spectral component with color temperature $\sim 1.7 - 1.8$ keV contributing $< 20\%$ to the total source flux in the 3-20 keV energy band (Fig. 3, 4). The monotonic rise of the source X-ray flux from $\sim 4 \times 10^{-9}$

Table 4. Summary of the source behavior for different states.

State	when observed	F_{total}^a	PL slope ^b	E_{cut}^c , keV	f_{soft}^d	rms_{total} , %	QPO
Rise phase	Feb 9–11, 98	4–12	1.7–2.2	60–70	< 20 %	12–28	2.5–4 Hz (5–15%)
Very high	Feb 12–18 (<i>Plateau 1</i>)	12–15	2.2–2.5	>200	14–22 %	10–11	4 QPOs in 0.06–14 Hz
	Feb 19–24 (<i>Plateau 2</i>)	17–20	2.5–2.7	>200	23–30 %	2–3.5	weak or no
	Feb 25–Mar 2 (<i>Plateau 3</i>)	10–11	2.3–2.4	>200	30–45 %	2–4	10–11 Hz (< 2%)
High ^e	Mar 12 – May 16	≤ 6	2.0–2.5	>200	> 50 %	<4	no or weak
Low ^e	after May 18, 98	≤ 1	1.5–2.0	50–100	< 10 %	>20	~0.1–1 Hz

^a – absorption corrected value of the total X-ray flux in the 3 – 20 keV energy range in units of $\times 10^{-9}$ erg s⁻¹ cm⁻²

^b – index of power-law approximation of hard component

^c – high-energy cut-off

^d – fraction of the soft spectral component flux in the 3 – 20 keV total flux

^e – only few typical observations for these states were analyzed

to $\sim 1.2 \times 10^{-8}$ erg/s/cm² § during this period was accompanied by gradual steepening of the hard spectral component and rise of the soft component flux (Fig. 4, Table 2).

The broad-band power density spectrum (PDS) of the source is dominated by strong band-limited noise (BLN) component and a complex of a relatively narrow QPO peaks ($\Delta f/f \sim 0.1 - 0.3$, where Δf and f are the width and the centroid frequency of the QPO peak) placed near the breakpoint in the slope of the BLN continuum (Fig. 5). For the first two observations (Feb. 9, 1998) the centroid frequencies of the QPO peaks are harmonically related, while for further observations this relation breaks. The evolution of the temporal properties of the source during this phase of the outburst is characterized by monotonic decrease of the total fractional rms amplitude of the rapid aperiodic variability from $\sim 28\%$ to $\sim 11\%$, accompanied by increase of the BLN break and QPO centroid frequencies (i.e. the systematic shift of the effective maximum of the power spectral density distribution to the higher frequencies; Table 3).

The complex of the X-ray properties of 4U1630-47 during this stage of the outbursts is very similar to that of some Galactic black hole candidates observed during their high-to-low and low-to-high state transitions (Tanaka & Lewin 1995). In fact, there are several general properties of the source showing that this state of the source does not match neither 'canonical' low nor high/very-high and probably corresponds to the transition between these states (see discussion below).

4.2 Very high state (VHS)

The peak of the 1998 outburst lasted for $\sim 25 - 30$ days and followed by an exponential decay. The peak itself can be roughly divided into three plateau at different flux levels, distinguished by the quantitative differences in the source spectral and temporal behavior.

§ – absorption-corrected value of the source X-ray flux in the 3 – 20 keV energy band

In spite of all these differences, the general complex of X-ray properties of the source during the whole period of peak flux allows to classify it as a 'canonical' very-high state established for Galactic black hole candidates (Miyamoto et al. 1991; Miyamoto et al. 1993; Tanaka & Lewin 1995).

Plateau 1. Total X-ray flux from the source detected with PCA rose slowly for observations ##6 – 26 with average level of $\sim 1.4 \times 10^{-8}$ erg/s/cm² (Fig 4). The broad-band energy spectrum in this state can be satisfactory described by the sum of two components: a relatively weak soft component (contributing < 20% to the total X-ray flux in the 3 – 20 keV energy band) with color temperature $\sim 1.6 - 1.7$ keV and a strong dominating hard component which has a power law form without high energy cut-off up to ~ 150 keV (Fig. 3).

The character of the X-ray variability of 4U 1630-47 during this period is of special interest. As it is clearly seen from the upper panel of Fig. 8, the light curve of the source is marked by presence of quasi-regular modulations with period of $\sim 10 - 20$ s. Similar variability was observed in the Galactic microquasars GRS 1915+105 (Morgan et al. 1997) and GRO J1655-40 (Remillard et al. 1999). See Fig. 8 and discussion in §5.2.

The broad-band PDS of 4U 1630-47 is strongly dominated by BLN component, total amplitude of the source rapid aperiodic variability in the 0.01 – 100 Hz frequency band was at the approximately constant level of $\sim 10\%$ (Fig. 5, Feb. 13 and 18 observations, Table 3). Two groups of QPO peaks are a generic feature of the source power density spectrum (Fig. 5, Table 3): first group located in the $\sim 0.05 - 0.2$ Hz frequency range, caused by aforementioned quasi-regular dipping and second group of QPO peaks at ~ 5 , ~ 7 and ~ 13 Hz. Contrary to the highly variable QPO features at ~ 5 and ~ 7 Hz, the 13 Hz QPO peak demonstrates relatively high stability of the centroid frequency and integrated rms amplitude (Table 3).

Plateau 2. Beginning on the Feb. 19 the flux from the source jumped up significantly and stayed high and variable until the observation #36 (Fig. 2). During this period the high energy part of the source spectrum be-

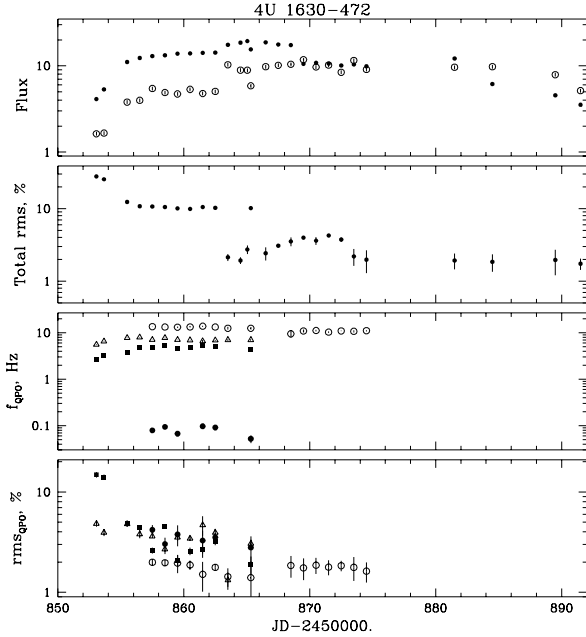


Figure 6. The evolution of main parameters of the source power density spectrum (three lower panels) along with the X-ray flux histories (upper panel). Filled and hollow circles in upper panel correspond to the total X-ray flux in the 3 – 20 keV energy range and the bolometric flux of the soft thermal component. 'Total rms' denotes the integrated fractional rms in the 0.01 – 128 Hz frequency range. Bottom panels show the evolution of the centroid frequency and integrated rms of various QPO components of the PDS.

came steeper, while the color temperature of the soft thermal component slightly rose to ~ 1.8 keV. Soft spectral component contribution was still below $\sim 30\%$ (Fig. 3, 4; Table 2), and its fast variability - significantly weaker (total rms variability $< 3\%$). QPOs became hardly detectable (Fig. 5, Feb. 20 observation). A notable exception was the observation #33, when source flux and behavior returned to the pattern of *Plateau 1*.

Plateau 3. Since the observation #36 (Feb. 24) the X-ray flux of 4U 1630-47 dropped to $\sim 1.1 \times 10^{-8}$ erg/s/cm² level and remained rather stable until the observation #44 (March 2). The quantitative characteristics of the broad-band energy spectra are quite different from that of the previous state: color temperature of the soft spectral component decreased to ~ 1.3 keV, the contribution of the soft component to the total X-ray luminosity increased up to the $\sim 40\%$ - level, while the high energy part of the spectrum significantly flattened (average photon index, $\alpha \sim 2.3$). The fractional variability of 4U 1630-47 somewhat increased (rms $\sim 4\%$). The PDS is dominated by BLN component with a peak at $\sim 1 - 2$ Hz, and, most notably, a prominent QPO feature with the frequency of $\sim 10 - 11$ Hz and rms amplitude $\sim 2\%$ showed up (Fig. 5, 6; Table 3). It should be noted, that this QPO feature again demonstrates relatively high stability of the centroid frequency and rms amplitude which allows us to treat it as a successor of the same nature as 13 Hz-QPO observed during the *Plateau 1*.

4.3 High state (HS)

After *Plateau 3* the flux from the source started to decline quasi-exponentially. Behavior of the source during the decline (after 19/03/1998 (observation #46) may be well described by standard high state of black hole candidates (see (Tanaka & Lewin 1995) for a review and references wherein).

4.4 Low state (LS)

At late stage of 1998 outburst the source underwent the transition from high to low state, which is also very typical for all Galactic black hole candidates and for X-ray Novae in particular. Hard power law spectrum was observed, in combination with rather strong fast variability at the level of $\sim 5 - 10\%$, and with QPO of variable frequency in the range $\sim 0.1 - 3$ Hz.

5 DISCUSSION

5.1 Spectral and timing properties of 4U 1630-47 during the rise phase of the outburst

We examined the 4U 1630-47 observations during the initial rise of 1998 outburst, and tried to understand how this state fits standard scheme of the 'canonical' states established for the black hole candidates (Tanaka & Lewin 1995). The broad-band energy and power density spectra of the source during this stage of the outburst are shown in Fig.7.

The energy spectrum is relatively hard ($\alpha \sim 2$) and has clear high-energy cut-off at the energies $\sim 60 - 70$ keV, the contribution of the soft thermal component to the total X-ray luminosity is small $< 20\%$. The same type of energy spectrum was previously observed during the initial rise phase of the outbursts of other X-ray Novae GS/GRS 1124-68 (Nova Muscae 1991; (Ebisawa et al. 1994; Takizawa et al. 1997)) and KS/GRS 1730-312 (Borozdin et al. 1995; Trudolyubov et al. 1996).

There is also a striking resemblance between the X-ray properties of 4U 1630-47 during the rise phase of the 1998 outburst and GRS 1915+105 in the low luminosity state (Trudolyubov, Churazov & Gilfanov 1999a). Corresponding broad-band energy and power density spectra of these sources are shown in Fig.7.

The spectrum and fast variability of 4U 1630-47 during this period is very similar to several Galactic black hole candidates, namely, Cyg X-1 (Belloni et al. 1996; Cui et al. 1997), GX 339-4 (Mendez & van der Klis 1996), GS 1124-68 (Miyamoto et al. 1994; Takizawa et al. 1997), GRO J1655-44 (Mendez, Belloni & van der Klis 1998), observed in the so-called intermediate state during their high-to-low and low-to-high state transitions. This state comprises properties of both low and very-high states and evidently corresponds to the transition between them. The X-ray flux of the source during the rise phase is significantly higher than in the typical low luminosity state $< 10^{-9}$ erg/s/cm². At the end of rise phase the flux is approaching the level very-high

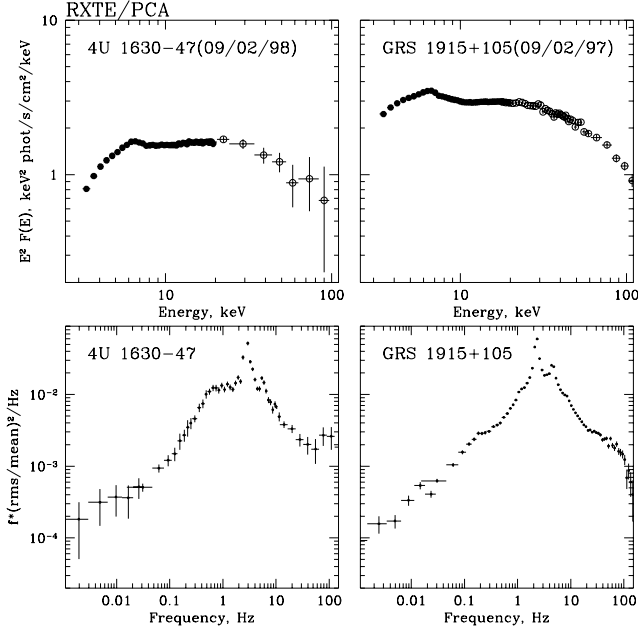


Figure 7. Demonstration of the similarity at the rise phase between 4U 1630-47 (*left panels*) and GRS 1915+105 (*right panels*). Energy spectra are presented in *upper panels*, and power density spectra – in *lower panels*.

state. As in low state, the spectrum is hard, furthermore, it exhibits high-energy cut-off, which is typical for low state, but not for very-high state.

While the energy spectrum resembles low state, the power density spectrum differs from the typical PDS in the low state: the frequency of the characteristic peak of the BLN continuum ($\sim 3 - 10$ Hz) is an order of magnitude higher than usual for Galactic black hole candidates in LS, but both general shape and characteristic frequencies of the PDS are consistent with that of the VHS.

The evolution of the spectral and timing parameters of 4U 1630-47 during the rise phase of the outburst can be generally understood in the framework of the two-phase model of the accretion flow around the compact object (i.e. the composition of a hot inner comptonization region (Sunyaev & Titarchuk 1980) and surrounding optically thick accretion disk (Shakura & Sunyaev 1973)). The interaction between these two distinct regions determines the properties of the spectrum and variability of the source. Assuming the QPO phenomenon to be related to the dynamical time scale on the boundary between the hot inner region and the outer accretion disk (Molteni, Sponholz & Chakrabarti 1996; Titarchuk, Lapidus & Muslimov 1998), we can treat the observed increase of the QPO centroid frequency as an indication of the inward motion of this boundary during the rise phase of the outburst. This interpretation is supported by simultaneous shift of the maximum of the PDS band-limited noise component (depending on the characteristic radius of the inner comptonization region) and softening of the energy spectrum. Aforementioned similarity between the rise of 4U 1630-47 1998 outburst and the outbursts of other

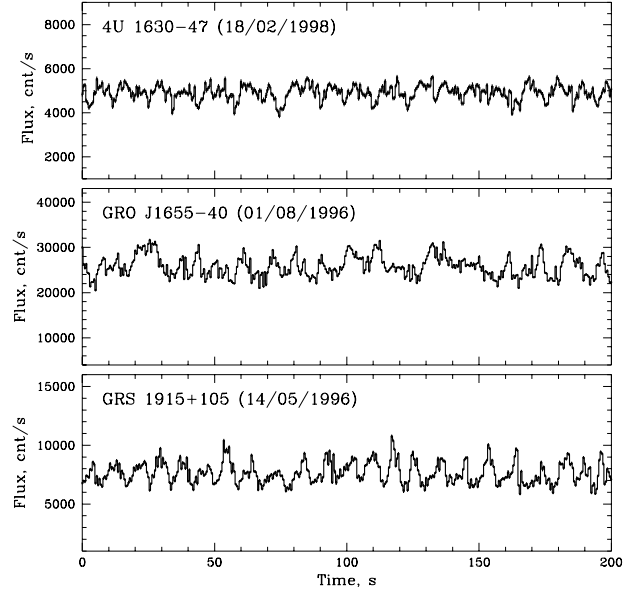


Figure 8. Similar X-ray variability patterns for 4U1630-47 (*upper panel*), GRO J1655-40 (*middle panel*) and GRS 1915+105 (*lower panel*) according to the RXTE/PCA observations (2 – 30 keV energy range, fluxes correspond to the 5 Proportional Counter Units).

X-ray Novae, allows us to suggest that in all these cases the approach of the inner edge of an optically thick accretion disk to the black hole causes the rise of the soft X-ray emission and softening of the broad-band energy spectrum. Alternatively, the hardening of the energy spectrum and decrease of the QPO centroid frequency and frequency of the BLN component maximum observed during the final stages of the X-ray Novae outbursts (Miyamoto et al. 1994; Mendez, Belloni & van der Klis 1998), could be explained in terms of the outward motion of the boundary between the inner region and an optically thick accretion disk.

5.2 Quasi-regular variability in 4U 1630-47 on time scales of tens of seconds

The variability of spectral and timing properties of the source during the *Plateau 1* is of special interest. As it is clearly seen from Figure 8 (upper panel), the light curve of the source is marked by presence of quasi-regular modulations with period $\sim 10 - 20$ s. This type of variability is seen in the PDS as a QPO peak in the range $0.05 - 0.1$ Hz showing harmonic content (see Table 3). We have performed detailed analysis of the variability of spectral and fast timing parameters of the source associated with this type of flux variability. All observations in *Plateau 1* were used for this analysis. We extracted energy and power density spectra of the source separated according to the level of the source energy flux using the data in the 'Binned' and 'Event' modes. The data were segregated according to the total count rate averaged over 2s time intervals. The range from minimum to maximum flux was divided into eleven equal parts.

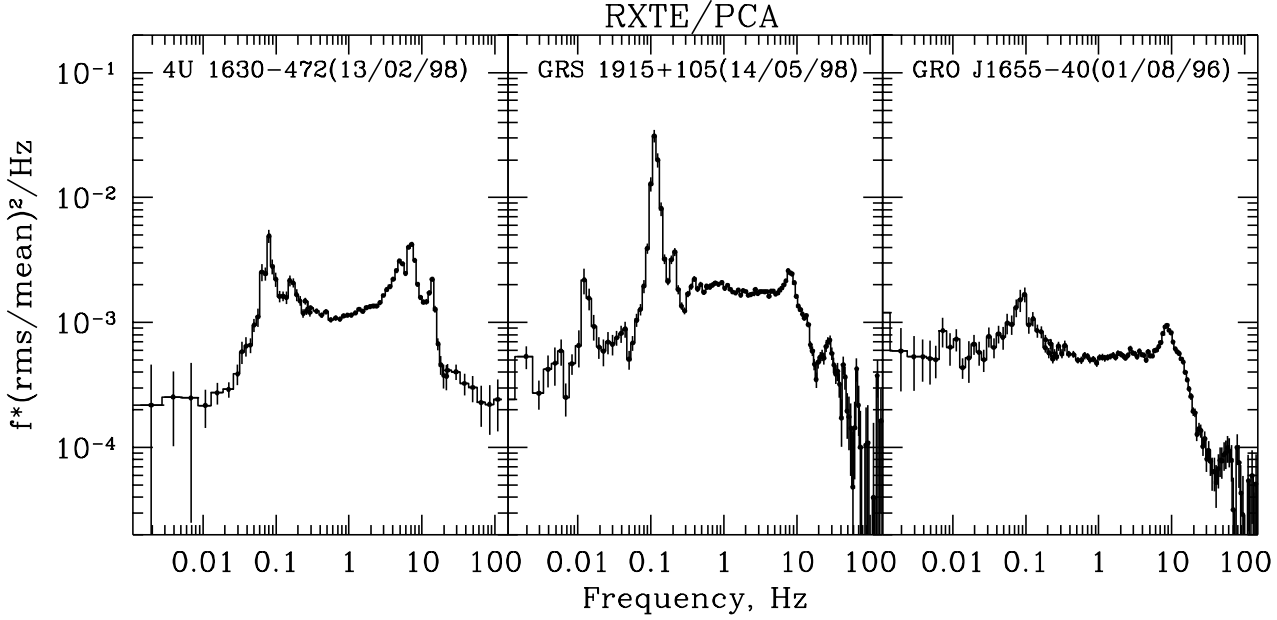


Figure 9. Power density spectra of 4U 1630–47, GRO J1655–40 and GRS 1915+105 for the observations with similar slow variability pattern (Fig. 8) PCA data.

Table 5. Main spectral parameters of 4U 1630–47 corresponding to the low and high flux levels, derived using the combination of the multicolor disc blackbody and power law models with correction to the interstellar absorption, fixed at the value of $8 \times 10^{22} \text{ cm}^{-2}$. (observation # 24 (18/02/1998), PCA data, 3–20 keV energy range). Parameter errors correspond to 1σ confidence level for the assumed 1% systematic uncertainty of data.

	T_d , keV	α_{pl}	f_{total}^a	f_{soft}^b	χ^2
Low	1.65 ± 0.06	2.27 ± 0.11	1.20	0.29	34.8(21)
High	1.91 ± 0.20	2.52 ± 0.13	1.62	0.35	29.2(21)

^a – absorption corrected value of the total X-ray flux in the 3–20 keV energy range in units of $\times 10^{-9} \text{ erg s}^{-1} \text{ cm}^{-2}$

^b – absorption corrected value of the soft spectral component flux in the 3–20 keV energy range in units of $\times 10^{-9} \text{ erg s}^{-1} \text{ cm}^{-2}$

PDS corresponding to each luminosity interval was fitted to the analytical model consisting of a band-limited component and up to three Lorentzians. Energy spectra were approximated by a multicolor disk plus power law model with correction to the low energy absorption. Energy spectra and PDS for the highest and the lowest flux intervals are presented in Fig. 10, 11.

There is a significant difference between the energy spectra of the source during the periods of the low and high flux: the rise of the X-ray flux is accompanied by softening of the hard spectral component and increasing of the effective temperature of the soft spectral component (Table 5, Fig. 10).

The properties of the source power density spectra corresponding to the periods of high and low flux are quite different. Low flux PDS has relatively high level of the total rms variability amplitude of $\sim 6.7\%$ (1–128

Hz frequency band) and is characterized by the presence of two prominent QPO features at ~ 4.5 Hz and ~ 13 Hz (Fig. 11, 12). The increase of the source flux is accompanied by drastic changes in the properties of the PDS: the 13-Hz QPO feature disappears, while the lower frequency QPO peak shifts to $\sim 6–7$ Hz (Fig. 11, 12). In addition, high flux PDS has much lower total rms amplitude of $\sim 3.5\%$ (1–128 Hz frequency band).

It is notable that somewhat similar type of variability was observed in Galactic microquasars GRS 1915+105 and GRO J1655-40 (Morgan et al. 1997; Remillard et al. 1999); see Fig. 8, 9. We speculate that this mode might be common for black hole binaries emitting at certain luminosity level. It is remarkable that in all cases, this mode corresponds to a relatively narrow interval of source luminosities. For 4U 1630–47 this type of variability was observed only for the *Plateau 1* observations, disappearing during the neighboring *Plateau 2* and *Plateau 3*. Moreover, when in the middle of the *Plateau 2* the source flux dropped to the level of *Plateau 1*, the pattern of variability immediately returned back (Table 3, observation #33).

5.3 Correlation between the spectral and timing parameters

Our analysis demonstrates a strong correlation between the energy spectrum of the source and its fast variability. During the initial rise of the outburst, and subsequent very-high state, the rise of the flux is accompanied by an increase of the QPO frequency, and decrease of the fast variability. For each plateau a stable flux level corresponds to stable spectral and timing parameters (Fig. 4, 6). It should be noted, that the complex

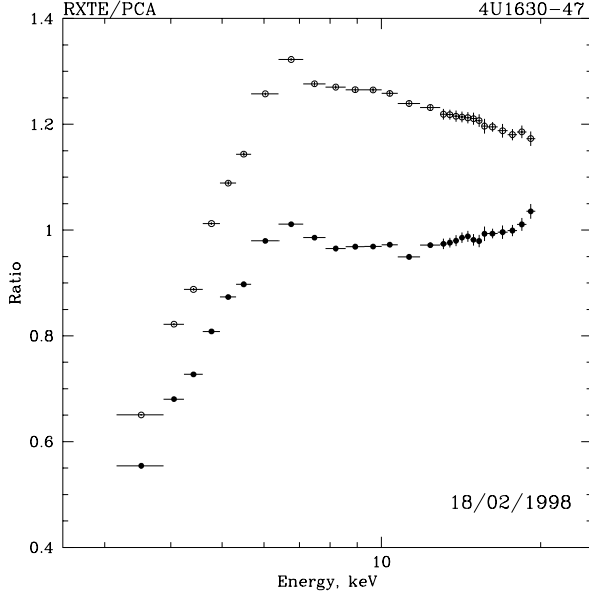


Figure 10. The changes in 4U1630-47 energy spectrum between the low (filled circles) and high (open circles) flux episodes for the same observation on *Plateau 1* (observation #24). Ratios of energy spectra to a power law with photon index $\alpha = 2.5$ are shown. The differences in both the temperature of soft component and the slope of hard component (also Table 5) can be interpreted as an inward motion of the accretion disk inner edge during the periods of higher flux.

of spectral and timing properties of 4U 1630-47 is very sensitive to the source luminosity level: changes of the source flux are accompanied by the changes in the energy spectrum and PDS. As an example, observation # 33 in the middle of *Plateau 2* has a flux typical of *Plateau 1*, and also *Plateau 1* spectral and temporal behavior.

We note the correlation of the total source fractional variability with the flux of the hard spectral component and with the total X-ray flux integrated over 2 – 30 keV band during the initial rise and maximum phase of the outburst (*Plateaus 1 and 2*). A similar correlation was first observed for GS/GRS 1124-68 (Nova Muscae 1991; Miyamoto et al. 1994) and later for many other Galactic black hole candidates.

The combination of the hot, optically thin quasi-spherical inner corona surrounded by outer optically thick accretion disk is considered nowadays as a plausible geometry for accretion onto a black hole (see e.g. (Dove et al. 1997)). A shock front formation between these two parts of the accretion flow is recognized as essential component of the picture in some models (Chakrabarti & Titarchuk 1995). We believe, that such models are able to reproduce qualitatively the correlations of spectral and timing properties observed for 4U 1630-47.

It is often suggested that the QPO phenomenon is caused by interaction between the two aforementioned distinct parts of the accretion flow, and occurs on the dynamical time scale at the boundary of

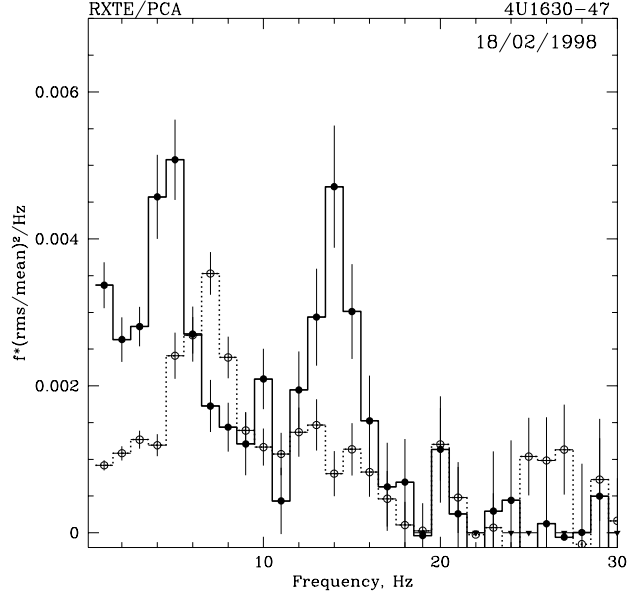


Figure 11. Comparison of the source power density spectra in units of frequency $\times (\text{rms}/\text{mean})^2/\text{Hz}$ during the low (filled circles, solid lines) and high (hollow circles, dotted lines) flux episodes for the same observation on *Plateau 1* (observation #24, 2 – 13 keV). QPO at ~ 13 Hz is prominent for low fluxes, and disappears for high fluxes. This may be attributed to the break-through of the shock, or to inward motion of the accretion disk (see the text).

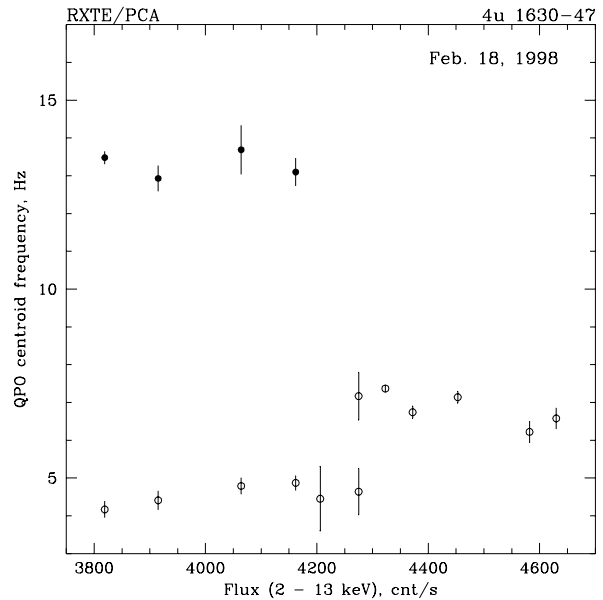


Figure 12. Dependence of the QPO centroid frequencies on the source flux in the 2 – 13 keV energy band (5 PCUs of PCA detector) for the Feb. 18 observation (#24). The ~ 13 -Hz QPO feature is not detectable for fluxes above ~ 4200 cnt/s. The centroid of the second QPO feature is jump-shifted to higher frequencies at the same flux level. These data may be interpreted as an existence of two distinct quasi-stable states with sharp transition between them.

these regions (Molteni, Sponholz & Chakrabarti 1996; Titarchuk, Lapidus & Muslimov 1998). Therefore, the change of the QPO centroid frequency is readily interpreted as an indication of the change in the effective radius of the boundary, which in turn is directly linked to the luminosities of the soft and hard components of the energy spectrum, and with the overall shape of energy spectrum.

Let us discuss the correlated fast and slow variability and spectral evolution, observed in 4U 1630-47 during the *Plateau 1* (see section §5.2), in the framework of this model. The observation of 13-Hz QPO only at lower fluxes shows that the structure associated with this QPO is present when flux level is low, and disappears or substantially weakens for higher fluxes. It is plausible that this structure might be a shock (Chakrabarti & Titarchuk 1995; Molteni, Sponholz & Chakrabarti 1996). Then the 13-Hz QPO could be caused by resonance oscillations of the shock, while the slow oscillations on the time scale of 10 – 20 s would correspond to the time of matter accumulation at the shock front (i.e. the shock stability time scale). A sudden breakthrough of the matter through the shock, or inward drift of the shock front leads to the disappearance of the 13-Hz QPO in PDS, or to the increase of QPO centroid frequency with simultaneous decrease of its strength below the threshold of our detection. The accompanying inward drift of the inner boundary of the accretion disk causes the increase of the centroid frequency of the second (4–8 Hz) QPO peak in PDS, and the increase of the soft component flux in agreement with observations (Fig. 10). The softening of the high energy part of the spectrum is probably caused by the increase of Thomson optical depth and decrease of the temperature of a hot corona behind the shock front. In fact, the accretion inside the shock in this case may be described also by a bulk motion Comptonization model (Chakrabarti & Titarchuk 1995; Titarchuk, Mastichiadis & Kylafis 1997). On the other hand, even in the absence of a shock, the source behavior could be explained by the movement of the boundary between the inner hot region and optically thick accretion disk caused by some kind of accretion disk instability (Titarchuk, Lapidus & Muslimov 1998; Trudolyubov, Churazov & Gilfanov 1999b).

The variations in the characteristic QPO frequencies hint at a change of some typical radius of the system, in particular, the inner radius of the optically thick accretion disk. Because the luminosity of the disk depends on both the accretion rate and the inner radius of the disk (Shakura & Sunyaev 1973), we can not simply attribute any changes in the source luminosity to the change of the accretion rate onto the central object. In fact, the luminosity can vary significantly for the same accretion rate, if the geometry of the system and relative contribution from disk and corona component change. The observation of several plateaus at the peak of the outburst shows the existence of some quasi-stationary modes of the accretion for this state. The high state, in contrast, exhibits a monotonic and quasi-exponential decrease, with associated spectral and temporal behavior changes.

5.4 Comparison with other outbursts

Of the three outbursts of 4U 1630-47 observed with the RXTE the outbursts of 1996 and 1999 look most similar. In both cases the flux from the source in ASM/RXTE energy band (1.3–12 keV) rose fast, was high and chaotically variable for some time, then faded quickly. The spectra at maximum were typical for the high state of Galactic black holes. The transition from high to low state was detected by the PCA and HEXTE during the 1999 outburst (McCollough et al. 1999). It is plausible that a similar transition would have been observed for the outburst of 1996, if pointed observations were available. Overall behavior of the source in these outbursts is that of a low-high-low state transitions, which is typical for "persistent" Galactic black hole binaries, namely, Cyg X-1 (Cui et al. 1998) and GX 339-4 (Belloni et al. 1999).

The outburst of 1998 was distinctly different from the other two observed from 4U 1630-47 by RXTE. It had a FRED-type light curve, with secondary maxima, as typical for X-ray transients (Chen, Shrader & Livio 1997). At the peak the source was in an unusual very high state, similar to what has been observed in X-ray Nova XTE J1748-288 (Revnivtsev, Trudolyubov & Borozdin 1999), and in the Galactic microquasars GRS 1915+105 (Morgan et al. 1997) and GRO J1655-40 (Remillard et al. 1999). So we see that the same source 4U 1630-47 demonstrates behavior seen in several Galactic binaries, which have one in common: all are black hole candidates. Observations of 4U 1630-47 confirm that all black hole systems have some similar X-ray properties, independent on the type of optical companion (low mass dwarves for X-ray Novae or early-type giant for Cyg X-1), and on long-term flux behavior (persistent, transient or chaotically variable). 4U 1630-47 may be considered as an intermediate case connecting different types of black hole binaries.

6 CONCLUSIONS

We analyzed the variability and spectral evolution of X-ray recurrent transient source 4U 1630-47 during its 1998 outburst. The RXTE satellite has observed three outbursts from this source to date. The behavior of the source during 1998 outburst differed significantly from previous outburst in 1996 and from the following one in 1999. While the interval between 1996 and 1998 outbursts was the same as between other consecutive outbursts observed in 1987–1996 (Kuulkers et al. 1997), the 1999 outburst happened much earlier than was expected (McCollough et al. 1999). We suggest that recurrence period of the system is not linked with its orbital period, but depends instead on the time of matter accumulation in outer accretion disk.

Light curve of 1998 outburst was of FRED-type typical for black hole X-ray Novae (Chen, Shrader & Livio 1997). Pointed observations by RXTE provided good coverage of all stages of the outburst from the rise of X-ray flux until late into the decline. We concentrated our analysis on the rise and maximum phases.

During the rise, the source demonstrated an interesting stage which can be considered as a transition between low/hard and very high state. The energy spectrum of the source was hard with an exponential high energy cut-off, similar to low state, while its fast variability was of the type more typical for VHS. We note that a similar energy spectrum was observed during rise phase from X-ray Novae GS/GRS 1124-68 (Ebisawa et al. 1994), KS 1730-312 (Trudolyubov et al. 1996), and for the low luminosity state of GRS 1915+105 (Trudolyubov, Churazov & Gilfanov 1999a).

The maximum of the outburst was divided into three plateaus, with almost constant flux within each plateau, and fast jumps between them. The spectral and timing parameters were also quite stable for each individual plateau, but distinctly different between the plateaus. The variability detected on the first plateau is of special interest. The source exhibits quasi-regular modulations with period of $\sim 10 - 20$ s during these observations. A similar type of variability was observed for both known Galactic microquasars GRS 1915+105 (Morgan et al. 1997) and GRO J1655-40 (Remillard et al. 1999). This variability holds for rather narrow range of luminosity for each source, which is known fact for the aforementioned microquasars, and was confirmed also by our observations for 4U 1630-47. Our analysis revealed significant differences in spectral and temporal behavior of the source at high and low fluxes during this period of time. The changes observed can be generally explained in the framework of the two-phase model of the accretion flow, involving a hot inner comptonization region and surrounding optically thick disk.

The evolution of 4U 1630-47 during the 1998 outburst is analogous to what was observed from other X-ray transients, namely, GS/GRS 1124-68 (Nova Muscae 1991; (Ebisawa et al. 1994)), KS 1730-312 (Borozdin et al. 1995; Trudolyubov et al. 1996), GRS 1739-278 (Borozdin et al. 1998), XTE J1748-288 (Revnivtsev, Trudolyubov & Borozdin 1999) and XTE J1550-564 (Cui et al. 1999). Near the peak of the outburst each showed an unusual very hard state dominated by a hard power law. This state is an addition to the canonical picture for these systems.

The other two outbursts observed with RXTE, in 1996 and 1999, resemble low-high-low state transitions observed from 'persistent' Galactic black holes GX 339-4 (Belloni et al. 1999) and Cyg X-1 (Cui et al. 1998). From the long-term flux history one may conclude that 4U 1630-47 is an intermediate between transients and persistent sources. As we discussed above, it demonstrates also states similar to the Galactic microquasars. Both high-mass binaries, as Cyg X-1, and low-mass binaries, as X-ray Novae, demonstrate similar spectral and temporal behavior, with several distinct states and transitions between them. We suggest that the accretion process and the generation of X-rays in all those systems has generic features attributable to their black hole nature.

7 ACKNOWLEDGMENTS

The research has made use of data obtained through the High Energy Astrophysics Science Archive Research Center Online Service, provided by the NASA/Goddard Space Flight Center.

REFERENCES

- Belloni, T., Mendez, M., Van der Klis, M., Hasinger, G., Lewin, W. H. G., & Van Paradijs, J. 1996, *ApJ*, 472, L107
- Belloni T., Mendez M., Van der Klis M., Lewin W.H.G., Dieters S., 1999, *ApJ*, 519, L159
- Borozdin K. N., Aleksandrovich N. L., Arefiev V. A., Sunyaev R. A., Skinner G. K., 1995, *Astr.L.* 21, 212
- Borozdin K. N., Revnivtsev M. G., Trudolyubov S. P., Aleksandrovich N. L., Sunyaev R. A., Skinner G. K., 1998, *Astr.L.* 24, 435
- Bradt H., Swank J., & Rothschild R., 1993, *A&AS*, 97, 355
- Callanan P. J., Charles P. A., Honey W. B., and Thorstensen J. R., 1992, *M.N.R.A.S.*, 259, 395
- Chakrabarti S. K., Titarchuk L. G., 1995, *ApJ*, 452, 226
- Chen W., Shrader C. R., Livio M., 1997, *ApJ*, 491, 312
- Cui W., Zhang S. N., Focke W., & Swank J. H., 1997, *ApJ*, 484, 383
- Cui W., Ebisawa K., Dotani T., Kubota A., 1998, *ApJ*, 493, L75
- Cui W., Zhang S. N., Chen W., & Morgan E., 1999, *ApJ*, 512, L43
- Dieters S., 1998a, *IAUC* 6823
- Dove J. B., Wilms J., Maisack M., & Begelman M. C., 1997, *ApJ*, 487, 759
- Ebisawa K., Ogawa M., Aoki T., Dotani T., Takizawa M., Tanaka Y., Yoshida K., Miyamoto S., Iga S., Hayashida K., Kitamoto S., Terada K., 1994, *PASJ*, 46, 375
- Jones C., Forman W., Tananbaum H., Turner M. J. L., 1976, *ApJ*, 210, L9
- Harmon B. A., Wilson C. A., Pasiesas W. S., and Pendleton G. N., 1994, *ApJ*, 425, L17
- Kaluzienski L. J., Boldt E. A., Holt S. S., Mushotsky R. F., 1978, *IAUC* 3197
- Kuulkers E., Parmar A. N., Kitamoto S., Cominsky L. R., and Sood R. K., 1997, *M.N.R.A.S.*, 291, 81
- Kuulkers E., Wijnands R., Belloni T., Mendez M., van der Klis M., and van Paradijs J., 1998, *ApJ*, 494, 753
- McCullough M. L., Harmon B. A., Dieters S., Wijnands R., 1999, *IAUC* 7165
- Mendez M., & van der Klis M., 1996, *ApJ*, 479, 926
- Mendez M., Belloni T., & van der Klis M., 1998, *ApJ*, 489, L187
- Mitsuda K., Inoue H., Koyama K., Makishima K., Matsuoka M., Ogawara Y., Suzuki K., Tanaka Y., Shibasaki N., Hirano T., 1984, *PASJ*, 36, 741
- Miyamoto S., Kimura K., Kitamoto S., Dotani T., Ebisawa K., 1991, *ApJ*, 383, 784
- Miyamoto S., Iga S., Kitamoto S., Kamado Y., 1993, *ApJ*, 403, L39
- Miyamoto, S., Kitamoto, S., Iga, S., Hayashida, K., Terada, K. 1994, *ApJ*, 435, 389
- Molteni D., Sponholz H., & Chakrabarti S. K., 1996, *ApJ*, 457, 805
- Morgan, E., Remillard, R., & Greiner, J. 1997, *ApJ*, 482, 993
- Muno M. P., Morgan E. H., & Remillard, R. A., 1999, to appear in *ApJ* (astro-ph/9904087)
- Narayan R. & Yi I., 1994, *ApJ*, 428, L13
- Parmar A.N., Stella L., & White N.E. 1986, *ApJ*, 304, 664
- Parmar A.N., Angelini L., & White N.E. 1995, *ApJ*, 452, L129
- Priedhorsky, W.C. 1986, *Ap&SS*, 126, 89

- Remillard, R., Morgan, E., McClintock, J., Bailyn, C., & Orosz, J. 1999, *ApJ*, 522, 397
- Revnivtsev M. G., Trudolyubov S. P., & Borozdin K. N., 1999, *MNRAS*, accepted (preprint astro-ph/9903306)
- Shakura N. I., Sunyaev R. A., 1973, *A&A*, 24, 337
- Shimura, T., & Takahara, F. 1995, *ApJ*, 445, 780
- Sunyaev R.A. & Titarchuk L.G., 1980, *A&A*, 86, 121
- Sunyaev R. A., Borozdin K. N., Aleksandrovich N. L., Arefiev V. A., Kaniovsky A. S., Efremov V. V., Maisack M., Reppin C., Skinner G. K., 1994, *Astr.L.*, 20, 777
- Takizawa, M., Dotani, T., Mitsuda, K., Matsuba, E., Ogawa, M., Aoki, T., Asai, K., Ebisawa, K., Makishima, K., Miyamoto, S., Iga, S., Vaughan, B., Rutledge, R., & Lewin, W. H. G. 1997, *ApJ*, 489, 272
- Tanaka Y., Lewin W. H. G., 1995, in *X-ray Binaries*, ed. W. Lewin, J. van Paradijs, E. van der Heuvel (Cambridge: Cambridge Univ. Press), 126
- Tanaka, Y., Shibazaki, N. 1996, *ARA&A*, 34, 607
- Titarchuk L., Lapidus I., & Muslimov, A. 1998, *ApJ*, 499, 315
- Titarchuk L. G., Mastichiadis A., Kylafis N. D. 1997, *ApJ*, 487, 834
- Tomsick J. A., Lapshov I., and Kaaret P., 1998, *ApJ*, 494, 747
- Trudolyubov, S.P., Gilfanov, M.R., Churazov, E.M., Borozdin, K.N., Aleksandrovich, N.L., Sunyaev, R.A., Khavenson, N.G., Novikov, B.S., Vargas, M., Goldwurm, A., Paul, J., Denis, M., Borrel, V., Bouchet, L., Jourdain, E., Roques, J.-P. 1996, *Astron. Lett.*, 22, 664
- Trudolyubov S., Churazov E., & Gilfanov M., 1999a, *Astron. Lett.*, 25, 827 (preprint astro-ph/9811449)
- Trudolyubov S., Churazov E., Gilfanov M., 1999b, *A&A*, 351, L15
- Vikhlinin A. A., Churazov E. M., & Gilfanov M. R., 1994, *A&A*, 287, 73
- Zhang W., Jahoda K., Swank J. H., Morgan E. H., & Giles A. B., 1995, *ApJ*, 449, 930